Development/Plasticity/Repair

Matched Pre- and Post-Synaptic Changes Underlie Synaptic Plasticity over Long Time Scales

Alex Loebel,[1]* Jean-Vincent Le Bé,[2]* Magnus J. E. Richardson,[3] Henry Markram,[2] and Andreas V. M. Herz[1]

[1]Faculty of Biology, Ludwig-Maximilians-Universität München, and Bernstein Center for Computational Neuroscience, D-82152 Munich, Germany, [2]Brain Mind Institute, Ecole Polytechnique Federale de Lausanne, CH-1015 Lausanne, Switzerland, and [3]Warwick Systems Biology Centre, University of Warwick, Coventry CV4 7AL, United Kingdom

Modifications of synaptic efficacies are considered essential for learning and memory. However, it is not known how the underlying functional components of synaptic transmission change over long time scales. To address this question, we studied cortical synapses from young Wistar rats before and after 12 h intervals of spontaneous or glutamate-induced spiking activity. We found that, under these conditions, synaptic efficacies can increase or decrease by up to 10-fold. Statistical analyses reveal that these changes reflect modifications in the number of presynaptic release sites, together with postsynaptic changes that maintain the quantal size per release site. The quantitative relation between the presynaptic and postsynaptic transmission components was not affected when synaptic plasticity was enhanced or reduced using a broad range of pharmacological agents. These findings suggest that ongoing synaptic plasticity results in matched presynaptic and postsynaptic modifications, in which elementary modules that span the synaptic cleft are added or removed as a function of experience.

Introduction

Synaptic transmission is essential for information processing in the nervous system, and long-term changes in synaptic properties are thought to be the physiological substrate of learning and memory (Goelet et al., 1986; Hebb, 1949; Martin et al., 2000; Ramón y Cajal, 1899). At the majority of synaptic connections, signal transmission relies on probabilistic release of presynaptic vesicles that induce quantal postsynaptic responses. Understanding how these key components change with neural activity has been the focus of intense research. One central finding concerns the different dynamics of these changes. Although long-term potentiation (LTP) of synaptic efficacies is initially expressed by increases of the postsynaptic responses, which require minutes to develop (Shepherd and Huganir, 2007; Südhof and Malenka, 2008), increases in the presynaptic number of release sites can take several hours (Bolshakov et al., 1997; Bayazitov et al., 2007). These observations led to the hypothesis that, over long enough time scales, the presynaptic and postsynaptic changes eventually match each other (Lisman and Raghavachari, 2006; Redondo and Morris, 2011). This hypothesis is supported by anatomical and functional attributes of synaptic connections that are observed at a single point in time: synapses with larger spines, which are associated with larger efficacies, have larger active zones that include more release sites (Schikorski and Stevens, 1997, 1999; Matsuzaki et al., 2001; Knott et al., 2006); and the smaller response variability of synapses with larger efficacies (Markram et al., 1997; Feldmeyer et al., 1999, 2002, 2006; Lefort et al., 2009; Loebel et al., 2009) is best explained by higher numbers of release sites and a quantal size (the postsynaptic response to one released vesicle) that is independent of the efficacy (Markram et al., 1997; Loebel et al., 2009).

Here, we explored the hypothesis that, over long time scales, LTP involves proportional presynaptic and postsynaptic modifications by examining the presynaptic and postsynaptic contributions to changes in synaptic efficacies after long periods of 12 h of spiking activity (Le Bé and Markram, 2006). The time span is long enough to capture modulations in the number of release sites, and whole-cell recordings from the same set of neurons at both ends of the 12 h period allowed us to monitor changes of the synaptic release parameters via quantal and failure analyses. We found that, by the second measurement phase, the synaptic connections had potentiated, or depressed, with a wide amplitude ratio of 0.08–14. The efficacy changes correlated strongly with the increase, or decrease, in the estimated number of release sites, whereas the quantal size remained unchanged. The relation between the presynaptic and postsynaptic components was not affected when the degree of synaptic plasticity expression was modulated by a broad range of pharmacological agents. Our findings provide strong evidence for a modular cross-synaptic nature of both long-term potentiation and long-term depression of synaptic efficacies and suggest that cortical synapses consist of elementary functional modules that span the synaptic cleft.

Materials and Methods

Electrophysiological recordings. The experimental procedures were previously described by Le Bé and Markram (2006). In summary, sagittal somatosensory cortical slices were obtained from young (postnatal day 12–14) Wistar rats of either sex and then perfused with 35°C ACSF (containing 125 mM

Received Aug. 5, 2012; revised Jan. 14, 2013; accepted Feb. 6, 2013.

Author contributions: A.L., J.-V.L.B., and H.M. designed research; A.L., J.-V.L.B., and M.J.E.R. performed research; A.L., M.J.E.R. and A.V.M.H. analyzed data; A.L., M.J.E.R., J.-V.L.B. and A.V.M.H. wrote the paper.

The authors declare no competing financial interests.

*A.L. and J.-V.L.B. contributed equally to this work.

Correspondence should be addressed to Dr. Alex Loebel, Faculty of Biology, Ludwig-Maximilians-Universität München, Großhaderner Straße 2, D-82152 Planegg-Martinsried, Germany. E-mail: alex.loebel@gmail.com.

DOI:10.1523/JNEUROSCI.3740-12.2013

 0270-6474/13/336257-10$15.00/0

NaCl, 2.5 mM KCl, 25 mM D-glucose, 25 mM $NaHCO_3$, 1.25 mM NaH_2PO_4, 2 mM $CaCl_2$, and 1 mM $MgCl_2$) throughout the experiment. Somatic whole-cell recordings were made using patch pipettes containing 100 mM potassium gluconate, 10 mM KCl, 4 mM ATP-Mg, 10 mM phosphocreatine, 0.3 mM GTP, 10 mM HEPES, and 5 mg/ml biocytin (pH 7.3, 310 mosmol/liter, adjusted with sucrose). Clusters of six or seven thick tufted layer-5 pyramidal cells were patched a first time ("before" phase), and their connectivity was recorded by using a stimulus train of eight action potentials at 30 Hz followed by a recovery test spike 500 ms later. The stimulation was repeated 30 times. Within 20 min the pipettes were withdrawn, and the slice was left in the recording chamber under various conditions (described below) for 12–14 h. The set of cells were then repatched, and the same stimulation protocol was executed to monitor their connectivity ("after" phase). After recording, the slices were fixed and ABC-stained; and because biocytin was used in the first and second patchings, we could double-check that the same cluster was patched for each experiment. The condition of slices at 12 h was excellent, with high visibility, no change in patchability (reflecting slice health), normal break-in resting potentials, normal discharge behavior, and no change in input resistances.

We considered the following experimental conditions: Control, included only the perfusion of ACSF; "Local glutamate," included ACSF in the presence of puffs of 50 mM sodium glutamate (Sigma-Aldrich) 100 μm above the cell cluster (the puffs were of 2 s duration every minute); and "Global glutamate," which included ACSF perfused with 100 μM sodium glutamate. In the following antagonist conditions, the slice was perfused with ACSF containing the antagonist concentrations described, and the glutamate was applied as in Local glutamate: 0.5 μM tetrodotoxin, a sodium channel blocker (TTX, Alomone Labs); 20 μM CNQX, an AMPA receptor antagonist (Sigma-Aldrich); 20μM D-2-amino-5-phosphonopentanoic acid, an NMDA receptor antagonist (D-AP5, Tocris Bioscience); 4 μM MPEP, an mGluR5 antagonist (Tocris Bioscience); 100 μM (2S)-α-ethylglutamic acid, a group II metabotropic glutamate receptor antagonist (EGLU, Tocris Bioscience); 20 μM (RS)-α-cyclopropyl-4-phosphonophenylglycine (CPPG), a group III mGluR antagonist (Tocris Bioscience); 50 μM O-phospho-L-serine (LSOP), a group III mGluR agonist (Tocris Bioscience). Finally, several experiments were performed in which spiking activity was induced by puffing 1 M KCl above the cluster. All animal experiments were done under the authorization no. 1550 of the Service Vétérinaire de l'Etat de Vaud.

The quantal model and the estimation of the quantal parameters. We considered a quantal model of synaptic transmission that accounts for short-term depression (Fuhrmann et al., 2002; Loebel et al., 2009). A synaptic connection is composed of N independent release sites, and from each release site a single vesicle, at most, is released with a probability p upon arrival of a presynaptic action potential. Subsequently, the vesicle contributes a quantum q to the postsynaptic response. Short-term depression is included by considering that, after vesicle release, the corresponding site remains empty until it is refilled with a new vesicle. The stochastic differential equation that describes these two processes of release and recovery is as follows:

$$\frac{d\sigma_i}{dt} = -\sigma_i \cdot r_i \cdot \delta(t - t_{sp}) + (1 - \sigma_i) \cdot \delta(t - t_{rec}) \quad (1)$$

where σ_i is the stochastic variable that represents whether a vesicle is present ($\sigma_i = 1$ with a probability ρ) or absent ($\sigma_i = 0$ with a probability $1 - \rho$) from release site i, r_i is the stochastic variable that represent whether a vesicle is released ($r_i = 1$ with a probability p) or not ($r_i = 0$ with a probability $1 - p$) at the time of a spike $t = t_{sp}$, and t_{rec} is a Poisson point process with rate $1/\tau_{rec}$, that is, the probability of refilling at any time interval dt is dt/τ_{rec}. The function $\delta(t)$ denotes the Dirac δ function, and the product $\Delta(t) \cdot \delta(t)$ leads to $x(t_{sp}^+) \rightarrow x(t_{sp}^-) + \Delta(t_{sp}^-)$ whenever a spike occurs (t_{sp}^- and t_{sp}^+ are the times just before and after a spike). The stochastic postsynaptic current, $I_{syn}(t)$, is described as follows:

$$\frac{dI_{syn}}{dt} = -\frac{I_{syn}}{\tau_{syn}} + q \cdot n_r \cdot \delta(t - t_{sp}) \quad (2)$$

where $n_r = \sum_{i=1}^{N} \sigma_i(t_{sp}) \cdot r_i(t_{sp})$ is the overall number of vesicles released at $t = t_{sp}$, and τ_{syn} is the current decay time constant. Completing the model is the equation for the membrane potential of the postsynaptic neuron:

$$\tau_{mem} \frac{dV}{dt} = -V + R_{in} I_{syn} \quad (3)$$

where τ_{mem} is the membrane time constant and R_{in} is the input resistance.

Averaging Equations 1–3 over the stochastic processes of release and recovery for a given spike train $\{t_{sp}\}$, while recognizing that σ_i and r_i are independent, yields the following deterministic equations (Gardiner, 1983):

$$\frac{d\rho}{dt} = \frac{1 - \rho}{\tau_{rec}} - p \cdot \rho \cdot \delta(t - t_{sp}) \quad (4)$$

$$\frac{dI_{syn}}{dt} = -\frac{I_{syn}}{\tau_{syn}} + A \cdot p \cdot \rho \cdot \delta(t - t_{sp}) \quad (5)$$

where ρ is the average occupancy $< \sigma_i >_{r_i, t_{rec}}$ of a release site and A is the absolute synaptic efficacy, representing the synaptic response when all vesicles are released (i.e., $A = N \cdot q$). The equation for the voltage of the postsynaptic cell has the same form as Equation 3. For convenience, R_{in} was absorbed in A.

The parameters of the model were fitted to each synaptic connection in a two-step approach. First, τ_{syn}, τ_{mem}, A, p, and τ_{rec} were estimated from the average synaptic response: τ_{syn} and τ_{mem} from the time course of the recovery-test excitatory postsynaptic potential (EPSP), and the remaining parameters from comparing the amplitudes of the 9 EPSPs to an analogous set of amplitudes derived analytically from the deterministic equations (Tsodyks and Markram, 1997; Loebel et al., 2009). In the second step of the estimation process, τ_{syn}, τ_{mem}, p, and τ_{rec} were integrated in stochastic Monte-Carlo simulations of the synaptic connection, and simulated single traces were produced in response to the same stimulation protocol used in experiments (i.e., same spike train stimulus and number of repetitions). The coefficients of variation (CV) of the simulated and recorded EPSPs were then compared. In a single comparison iteration, a set of simulations were performed with an increasing value of N over a certain range (usually between 1 and 100, with the upper limit adjusted for the stronger connections), and the estimated value was the value that resulted in the minimum mean-least-square distance between the CVs of the simulated and recorded EPSPs (see Fig. 1*C*). Repeating this evaluation process for 100 iterations resulted in a distribution of values of the parameter N, which determined its expectation and confidence intervals (see Fig. 1*C*). The quantal size was then calculated as: $q = A/N$.

To provide a measure for the reliability of the estimates of the quantal parameters, we applied a nonparametric Bootstrap method (Efron and Tibshirani, 1993) to the synapses of the Global glutamate condition. This analysis provided 68 data points, as each synaptic connection was measured twice (at the "before" and "after" measurement phases). For each connection, 50 replica sets of single traces were constructed by randomly selecting with replacement traces from the original measured data, until the replica set had the same size as the measured set. The quantal analysis was applied to each replica sets, and from the 50 values for each synaptic parameter, means and SDs were calculated using Bootstrap-adjusted equations (Efron and Tibshirani, 1993). We found that the mean values for the parameters gathered from the bootstrap replica sets were very similar to the estimated values from the original dataset ($\bar{N}_{bootstrap}/N = 1.02 \pm 0.01$, $\bar{p}_{bootstrap}/p = 1.01 \pm 0.007$, and $\bar{q}_{bootstrap}/q = 0.99 \pm 0.01$, mean ± SEM, $n = 68$); and the CVs of the parameters within the bootstrap replica were $CV_p = 0.07 \pm 0.005$, $CV_q = 0.13 \pm 0.009$, and $CV_n = 0.14 \pm 0.009$, mean ± SEM, $n = 68$).

The uniformity assumption of the release parameters (i.e., that all release sites have the same probability of release and recovery time constants) has no bias on the estimation of the quantal parameters (Loebel et al., 2009). Other possible sources of variability (i.e., intersite and intrasite differences in quantal size, jitter in spike timing, and background noise) lead to our estimates of N to be conservative, with 10% underestimation on average (Loebel et al., 2009).

Direct amplitude measurement and failure analysis. To directly measure EPSP amplitudes and also count the number of failures, we first transformed the traces into well-separated pulses using a deconvolution

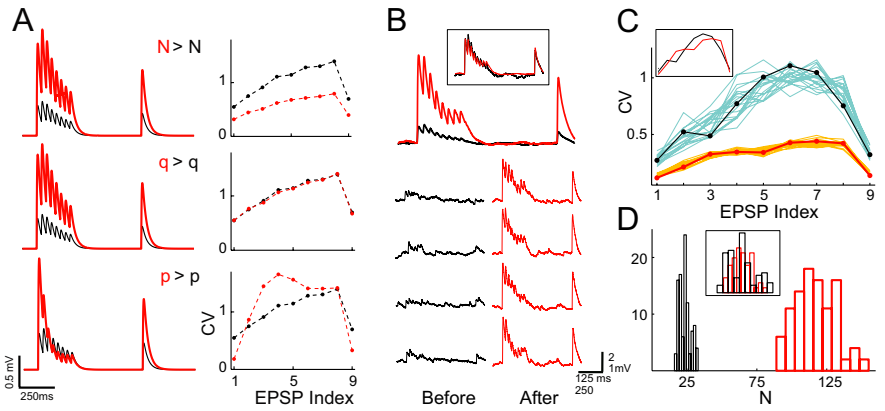

Figure 1. Matched presynaptic and postsynaptic changes in sLTP. ***A***, The quantal model predicts different changes in the temporal dynamics of the average response to a presynaptic spike train (left column), and in the response variability profile (right column), when increasing any one of the three parameters, N, q, or p. Here, the increase was by a factor of 3 (in red). Initial values for the parameters were as follows: $N = 10$, $p = 0.25$, and $q = 0.2$ mV. The recovery time constant was kept at $\tau_{rec} = 500$ ms in all simulations. The "EPSP index" labels the nine synaptic responses to a spike train with 8 action potentials at 30 Hz followed by a single spike after 500 ms. ***B***, Representative single traces (bottom), and averages (top), of an example synaptic connection before and after sLTP was induced. Inset, Scaling the response amplitudes indicates that the temporal dynamics of the average response did not change. ***C***, The CV of all of the nine synaptic responses exhibited a decrease in the "after" phase. Inset, The scaled CVs show no profile change. Light blue and orange represent best fits from 20 sets of Monte-Carlo simulations. ***D***, Histograms of the estimated number of release sites, derived from 100 sets of Monte-Carlo simulations for each of the measurement phases. Inset, The scaled distributions show that the confidence intervals for the means were similar both "before" and "after." ***B–D***, The same synaptic connection. The estimated parameters for this synapse is as follows: $N_{before} = 24 \pm 1$, $N_{after} = 117 \pm 2$ (mean ± SEM); $p_{before} = 0.41$, $p_{after} = 0.45$; $q_{before} = 0.088$ mV, $q_{after} = 0.086$ mV; $\tau_{rec,before} = 484$ ms, $\tau_{rec,after} = 396$ ms.

method (Richardson and Silberberg, 2008; Loebel et al., 2009) (see Fig. 5*A*). The method inverts the low-pass filtering resulting from the cell membrane by rearranging Equation 3:

$$R_{in} I_{syn} = \tau_{mem} \frac{dV}{dt} + V \quad (6)$$

The right-hand side of Equation 6 is evaluated using the voltage trace, its derivative, and τ_{mem}. The deconvolved pulses can be isolated and reconvolved by solving Equation 6 for the voltage with the resulting EPSP amplitudes measurable in the same way as for isolated EPSPs (Richardson and Silberberg, 2008; Loebel et al., 2009).

Comparing the amplitudes of the deconvolved mean synaptic response to the following equations, derived from Equations 4 and 5, yields A, p, and τ_{rec} as follows:

$$< \text{Amp} >^{\mu} = A \cdot p^{\mu} \quad (7)$$

$$\rho^{\mu+1} = \rho^{\mu} \cdot (1 - p) \cdot e^{-\frac{\Delta_{\mu}}{\tau_{rec}}} + 1 - e^{-\frac{\Delta_{\mu}}{\tau_{rec}}}, \rho^{1} = 1 \quad (8)$$

where $p^{\mu} = p \cdot \rho^{\mu}$ is the probability of a vesicle being released on arrival of the μ^{th} presynaptic pulse. The values of the parameters were consistent with those extracted directly from the voltage traces. Subsequently, an estimate of the number of release sites N can be obtained by counting the number of failures F^{μ} at the single traces and compare it with the expected failure probability for each pulse:

$$F^{\mu} = (1 - p^{\mu})^{N} \quad (9)$$

Failure rates can be estimated by comparing AP-triggered and background amplitude histograms (Isope and Barbour, 2002). In particular, normalizing the negative components of the background and AP-triggered EPSP distributions yields a multiplication factor that is equal to the failure rate. Here, we used a related approach to that of Isope and Barbour (2002), as our data comprised an insufficient number of sweeps to accurately match the amplitude histograms themselves. The failure rates were therefore estimated by considering negative AP-triggered voltage excursions as failures. This number was doubled to estimate the total number of failures. The latter step follows from the expected symmetry of voltage amplitude fluctuations around zero in the case of a release failure. This method gave estimates for N that were in excellent agreement with those calculated from the CV analysis (see Fig. 5*C*).

For completeness, we also estimated N from comparing the CV of the deconvolved synaptic responses with the model. In particular, the CV at the μ^{th} pulse was calculated by dividing the expected SD:

$$SD^{\mu} = \sqrt{q^2 \cdot N \cdot p^{\mu}(1 - p^{\mu}) + \text{Var}(\chi)} \quad (10)$$

by the mean $< \text{Amp} >^{\mu}$, given in Equation 7. Here, χ is the background noise as measured in a region away from the stimulated EPSPs. The values of N derived using this method were comparable with those estimated from the voltage traces in all cases examined (e.g., see Fig. 5*C*) (Loebel et al., 2009).

Results

To evaluate the changes in synaptic transmission properties during long stretches of ongoing neural activity, the connectivity within clusters of six or seven layer-5 thick tufted pyramidal neurons was measured using whole-cell patch-clamp, and the same experimental protocol was repeated after a 12 h period. Between the two patching sessions, the slices were either spontaneously active or spiking activity was induced by either puffing glutamate above the cluster (Local glutamate condition) or by adding glutamate to the bathing solution (Global glutamate condition) (see Materials and Methods). During both patching sessions, referred to as "before" and "after" the connectivity was probed by repeatedly stimulating the cells with a train of 8 action potential at 30 Hz followed by a single recovery action potential 500 ms later, a stimulus pattern that reveals the characteristic short-term depression dynamics of layer-5 excitatory synapses (Fig. 1). This experimental protocol allows one to detect the appearance and disappearance of synaptic connections, which may represent the synaptic rewiring of neocortical micro-circuits (Le Bé and Markram, 2006). Here, we focused on the synaptic connections that were found both "before" and "after." As shown by Le Bé and Markram (2006), the efficacy of most of these synaptic connections either increased (slow-LTP or sLTP) or decreased (sLTD) between the "before" and "after" measurement phases.

To determine which of the synaptic components (i.e., the number of release sites N, the probability of vesicle release p, or the quantal size q) underlies the changes in efficacy, we compared the synaptic responses with an extension of the classic quantal-release model (Del Castillo and Katz, 1954). The extended model (Fuhrmann et al., 2002; Loebel et al., 2009) captures the dynamics of short-term depression by considering that, once a vesicle is released, the corresponding release site remains empty until being refilled by a new vesicle (Thomson et al., 1993; Debanne et al., 1996; Varela et al., 1997; Silver et al., 1998; Zucker and Regehr, 2002). The average response of the quantal model to a presynaptic spike train is equivalent to the deterministic model of synaptic depression (Abbott et al., 1997; Tsodyks and Markram, 1997). Hence, the probability of release, the recovery time constant, τ_{rec} (the time governing the refilling process of an empty release site), and the absolute synaptic efficacy, A, can be estimated from the temporal dynamics of the average response of a synaptic connection (see Materials and Methods). The parameter A represents the expected response if all release

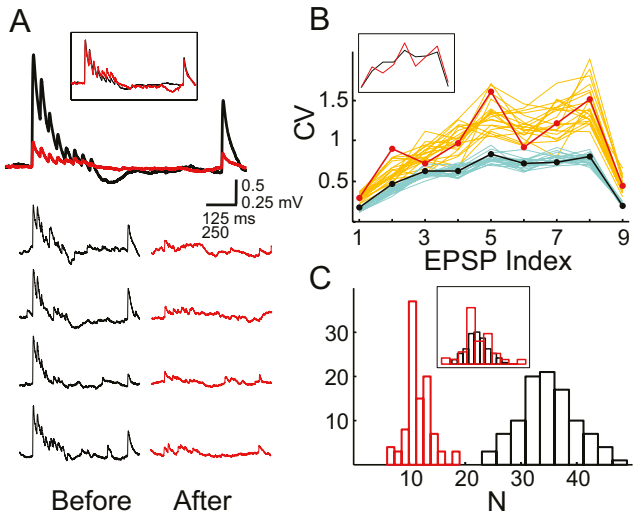

Figure 2. Matched presynaptic and postsynaptic changes in sLTD. ***A–C***, Sample traces, average responses, and CV analysis for a synaptic connection before and after sLTD was induced. As for sLTP (Fig. 1), the short-term dynamics of the average response and the CV profile did not change; and the change in efficacy was captured by a modulation of the number of release sites (here a decrease in N), and a similar quantal size. The estimated parameters for this synapse: $N_{before} = 35 \pm 1, N_{after} = 12 \pm 0.2$ (mean ± SEM); $p_{before} = 0.58, p_{after} = 0.5$; $q_{before} = 0.11$ mV, $q_{after} = 0.09$ mV; $\tau_{rec,before} = 543$ ms, $\tau_{rec,after} = 605$ ms.

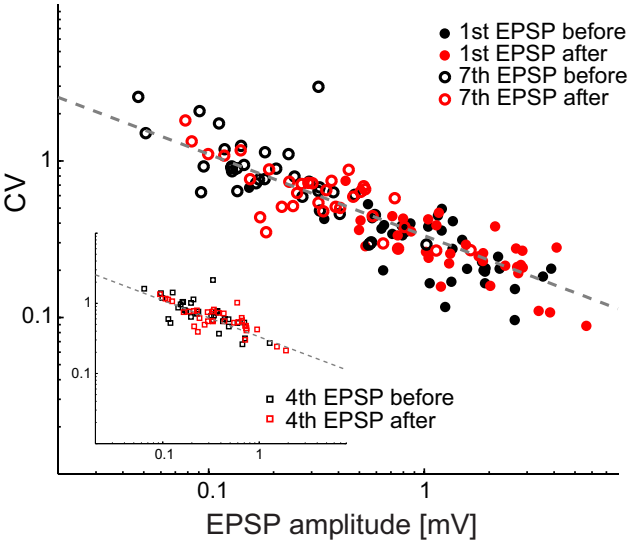

Figure 3. The relation between the mean EPSP and its CV is similar in the "before" and "after" phases. The CV of the responses to the spike train stimulus decreased as a power law of the mean response amplitude in both the "before" and "after" phases. Shown are the CV-mean relations of the first (filled circles), fourth (squares, inset), and seventh (circles) EPSPs of the connections from the Global glutamate experimental condition. The respective exponents of the power law relation were similar at both measurement phases: $\kappa_{before} = -0.49$ and $\kappa_{after} = -0.48$ for the 1st EPSP, $\kappa_{before} = -0.5$ and $\kappa_{after} = -0.46$ for the fourth EPSP, and $\kappa_{before} = -0.55$ and $\kappa_{after} = -0.48$ for the seventh EPSP. The exponents were remarkably similar to the value $\kappa = -0.5$ predicted from the quantal model (in gray). See Materials and Methods (Eqs. 7 and 8). Mean EPSPs were larger in the "after" phase, as in Figure 1A (top). In particular, the 1st EPSP increased from 1.41 ± 0.15 mV to 1.83 ± 0.21 mV, the fourth EPSP from 0.33 ± 0.042 mV to 0.48 ± 0.066 mV, and the seventh EPSP from 0.25 ± 0.034 mV to 0.41 ± 0.055 mV (mean ± SEM; $n = 34$).

sites were activated by an action potential (i.e., $A = N \cdot q$). The number of release sites can then be evaluated from comparing the CV of the measured responses of a connection with an analogous set obtained from Monte-Carlo simulations of the quantal model (see Materials and Methods). This two-step fitting algorithm was applied, independently, to the "before" and "after" measurements of each synaptic connection. The reliability of the estimated quantal parameters was confirmed by applying a bootstrapping method to data from the Global glutamate condition (see Materials and Methods).

There are two main advantages in our approach of using the short-term depression dynamics: all three quantal parameters can be evaluated from a single set of measurements (Loebel et al., 2009); and distinguishing between their contribution to the efficacy changes is straightforward. In particular, changes in release probability are predicted to result in a redistribution of the synaptic response efficacies within the spike train, whereas an increase in N or q leads to a uniform efficacy increase of all responses (Fig. 1*A*). The latter two parameters can be distinguished by comparing the variability of the responses "before" and "after"; the model predicts a decrease in the CVs if N increases, and no changes if q is modified (Fig. 1*A*). The scenario we repeatedly observed in our analysis is shown in Figures 1*B*, *C* and 2 via example synaptic connections. For comparison with previous studies of synaptic plasticity, we use the terms sLTP and sLTD when an increase, or a decrease, respectively, is observed in the 1st EPSP amplitude (defining sLTP and sLTD as a change of the absolute synaptic efficacy, i.e., the A parameter, led to the same results). In sLTP, synaptic responses in the "after" phase were stronger and less variable (Fig. 1*B*). The temporal dynamics of the mean responses "before" and "after" were quite similar, and the same was true for the CV profiles (Fig. 1*C*). Fitting the average responses yielded similar release probabilities ($p_{before} = 0.41$ and $p_{after} = 0.45$) and an increase in the absolute synaptic efficacy ($A_{before} = 2.1$ mV and $A_{after} = 10.1$ mV). The lower CVs of the synaptic responses in the "after" phase were explained by a higher estimate for the number of release sites, with $N_{before} = 24 \pm 1$ and $N_{after} = 117 \pm 2$ (mean ± SEM, from $n = 100$ sets of Monte-Carlo simulations; Fig. 1*D*). These values for N result in almost identical quantal sizes for both measurement phases ($q_{before} = 0.088$ mV and $q_{after} = 0.086$ mV). Thus, the observed increase in efficacy and decrease in response variability at this synaptic connection are consistent with an increase in the number of release sites, alongside postsynaptic changes that are reflected in a practically constant quantal size per release site. In sLTD we observed the opposite properties for the synaptic responses (i.e., they became weaker and more variable in the "after" phase; Fig. 2*A*, *B*). The temporal dynamics of the short-term depression was again similar in both measurement phases, resulting in similar release probabilities ($p_{before} = 0.58$ and $p_{after} = 0.5$). The decrease in efficacy and increase in response variability were explained by a decrease in the number of release sites ($N_{before} = 35 \pm 1, N_{after} = 12 \pm 0.2$, mean ± SEM; Fig. 2*C*). The release sites remaining in the "after" phase exhibited a quantal size similar to that of the "before" phase ($q_{before} = 0.11$ mV and $q_{after} = 0.09$ mV). Hence, sLTD is explained by a decrease in the number of release sites, alongside postsynaptic changes that maintain the quantal size. Comparing the dynamics of both synaptic connections suggests that sLTP and sLTD are the opposite expressions of a single underlying process.

A population analysis of the synaptic connections from the Global glutamate experiments supports the suggested relation between the quantal parameters and the observed sLTP and sLTD. In the "before" measurement phase, the amplitudes of the 1st EPSP responses ranged from 0.15 to 3.9 mV, with a population mean of 1.41 ± 0.25 mV (mean ± SEM; $n = 34$). The CV of these responses decreased as a power law function of the mean amplitude, with a fitted exponent of $\kappa = -0.49$ (Fig. 3). This value is remarkably similar to the value $\kappa = -0.5$ predicted from the quantal model if

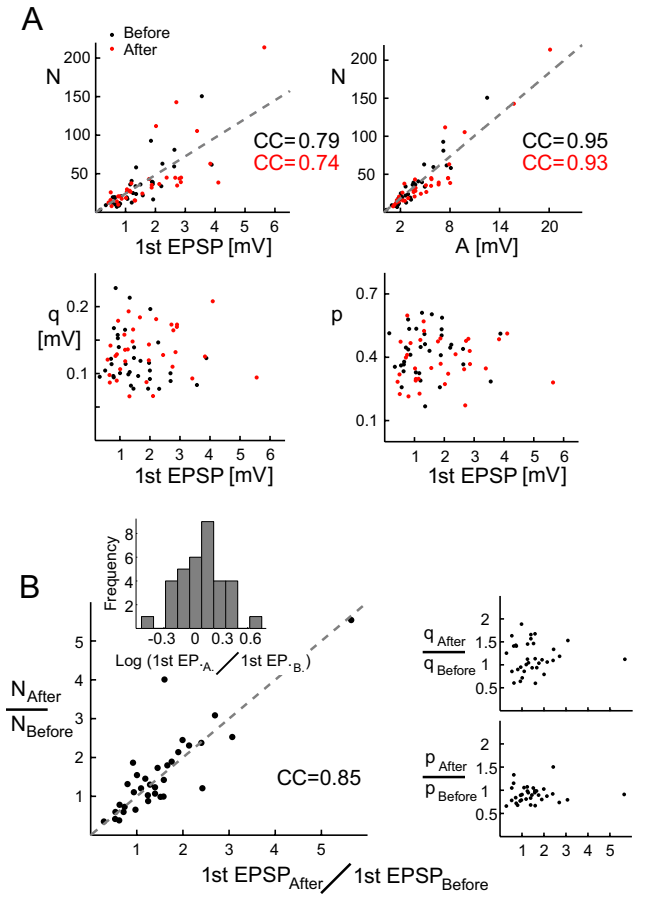

Figure 4. Population quantal analysis of the synaptic connections for the glutamate bathing experiments (Global glutamate condition). ***A***, Estimated quantal parameters ($n = 34$). Only the number of release sites correlated with the synaptic efficacy at both phases of measurement. ***B***, Plotting the relative change of the quantal parameters versus the respective amplitude ratio of the 1st EPSP reveals that only the number of release sites *N* is correlated with the observed sLTP or sLTD. Here, sLTP corresponds to 1st $EPSP_{after}$/1st $EPSP_{before} > 1$, and sLTD corresponds to 1st $EPSP_{after}$/1st $EPSP_{before} < 1$. Inset, The distribution of 1st $EPSP_{after}$/1st $EPSP_{before}$. The mean and SD are 1.5 ± 0.98. For clarity, the EPSP ratios are shown on a logarithmic scale.

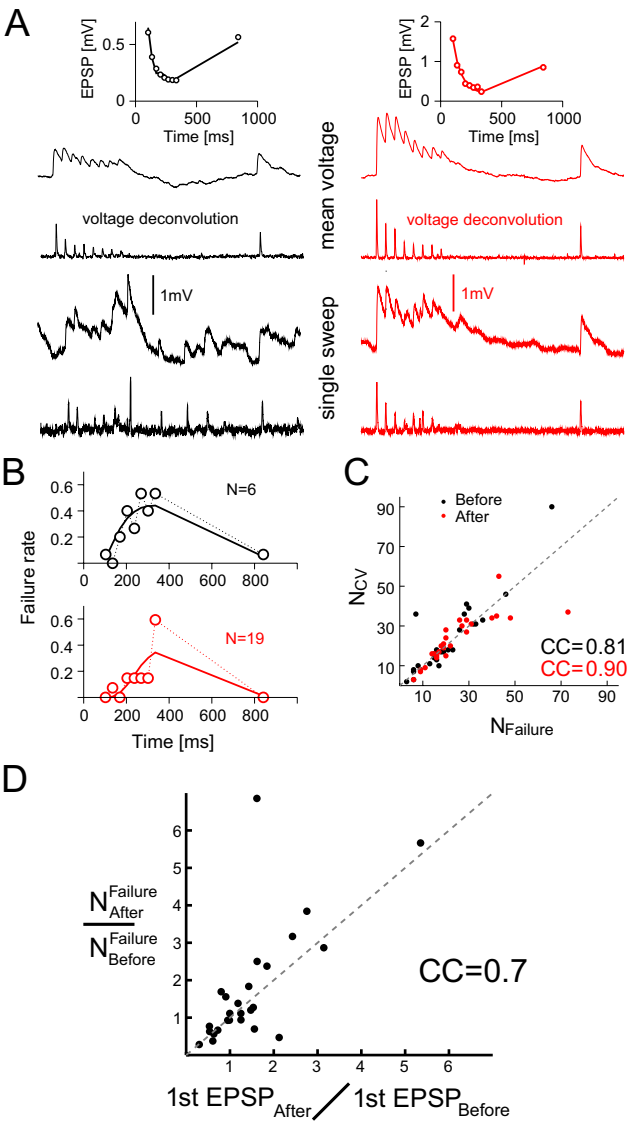

Figure 5. Direct EPSP measurement: CV and failure analysis. ***A***, The deconvolution method transforms average and single voltage traces to current-like traces. Top insets, Estimating the parameters that determine the temporal dynamics of the responses (e.g., the probability of release, from fitting Eqs. 7 and 8 to the amplitudes of the deconvolved mean traces). Empty circles represent data points; continuous lines indicate model fit; black and red traces, "before" and "after" phase, respectively. ***B***, The deconvolution of the single traces allows for the easier detection of failures. In the example shown, fewer failures were detected at the synaptic responses measured in the "after" phase, resulting in a higher *N* estimate. ***C***, The number of release sites was also estimated from the CV of the amplitudes of the deconvolved single traces (Eqs. 7, 8, and 10). The estimated *N* values from the two methods were remarkably similar. ***D***, The ratio of the number of release sites, which were estimated using the failure analysis, captures the change in the synaptic efficacy during sLTP and sLTD. Shown are the 25 connections (of 34) from the data in Figure 2, which were amenable to the failure analysis.

changes in *N* alone cause the efficacy differences between weak and stronger connections. By the second measurement phase, the connections strengthened on average, with a similar relative increase at the 1st EPSP response (to 1.83 ± 0.21 mV, mean ± SEM; $n = 34$, with a range of 0.43–5.6 mV) and at the other responses along the spike train. The CV-amplitude relations (Fig. 3) and the temporal dynamic of the average responses (data not shown) were also similar in the "before" and "after" phases. Together, the overall increase in the response amplitudes was captured by comparable increases in *A* and *N* ($A_{before} = 3.58 \pm 0.43$ mV, $A_{after} = 5.15 \pm 0.69$ mV, $N_{before} = 34 \pm 5$, $N_{after} = 43 \pm 7$, mean ± SEM; $n = 34$), and with similar release probabilities and quantal sizes ($p_{before} = 0.42 \pm 0.02$, $p_{after} = 0.38 \pm 0.02$, $q_{before} = 0.12 \pm 0.01$, $q_{after} = 0.13 \pm 0.01$, mean ± SEM; $n = 34$). All values, both "before" and "after," were comparable with those reported previously for this type of connection (Markram et al., 1997; Tsodyks and Markram, 1997; Richardson et al., 2005; Le Bé and Markram, 2006; Loebel et al., 2009). Significantly, of the three quantal components, only the values for the number of release sites N_{before} and N_{after} had the same relative range as, and were correlated with, the synaptic efficacies. As shown in Fig. 4*A*, this result did not depend on whether synaptic efficacies were measured by the amplitude of the 1st EPSP ($CC_{before} = 0.79$, $p < 0.001$; $CC_{after} = 0.74$, $p < 0.001$) or by *A*, the absolute synaptic efficacy ($CC_{before} = 0.95$, $p < 0.001$; $CC_{after} = 0.93$, $p < 0.001$, $n = 34$, *t* test). In particular, the intrasynaptic ratio N_{after}/N_{before} was strongly correlated with the ratio of the synaptic efficacies, both for potentiated and depressed synaptic connections (with 1st $EPSP_{after}$/1st $EPSP_{before}$, correlation coefficient [CC] = 0.85, $p < 0.001$, Fig. 4*B*; and with A_{after}/A_{before}, CC = 0.89, $p < 0.001$; data not shown; $n = 34$, *t* test). The intrasynaptic ratios of the probability of release and quantal size, on the other hand, were not correlated with the observed sLTP or sLTD (Fig. 4*B*). Furthermore, we did not observe any differences between sLTP and sLTD apart from the changes in *N*, with similar intrasynaptic ratio of the probability of

release and quantal size at sLTP and sLTD ($p_{after}^{sLTP} / p_{before}^{sLTP} = 0.92 \pm 0.04$ and $p_{after}^{sLTD} / p_{before}^{sLTD} = 0.88 \pm 0.06$, mean ± SEM, $p = 0.48$, two-sample t test; $q_{after}^{sLTD} / q_{before}^{sLTD} = 1.15 \pm 0.06$ mV and $q_{after}^{sLTD} / q_{before}^{sLTD} = 1.18 \pm 0.12$ mV, mean ± SEM, $p = 0.8$, two-sample t test; $n_{sLTP} = 23$, $n_{sLTD} = 11$).

Direct measurement of EPSPs and failure analysis

The number of transmission failures provides an additional insight into which synaptic components underlie the observed efficacy changes. For example, a decrease in the number of failures in the "after" phase is predicted to result from an increase in either N or p, whereas changes in q do not affect transmission failures (Eq. 9). Failure events can be straightforwardly identified using a deconvolution method (Fig. 5*A*) in which the membrane-time-constant filtering of the intracellular traces is removed (Richardson and Silberberg, 2008), leaving a signal with much higher temporal detail. The failure rates were subsequently calculated using a method related to that of Isope and Barbour (2002), as described in Materials and Methods. From the short-term dynamics of the deconvolved mean responses we estimated the probability of release, and from the single traces we calculated the CV of the responses and estimated the number of failures (see Materials and Methods). We previously showed that the two different approaches, voltage deconvolution and the CV-mean analysis described in the previous section, provide similar estimates for the parameters extracted from the mean amplitudes (p and τ_{rec}), and for the estimates for N from the response variability (Loebel et al., 2009).

The failure analysis is illustrated in Figure 5*A*, *B* for an example synaptic connection. In particular, the number of failures was substantially lower in the "after" phase; and as the probability of release was similar at "before" and "after" ($p_{before} = 0.42$, $p_{after} = 0.36$), the decrease in failures was fully captured by an increase in the number of release sites, with $N_{before} = 7$ and $N_{after} = 19$. The failure analysis was applicable to the majority of the connections from the Global glutamate experiments (25 of 34 connections; we disregarded traces in which the stimulation artifacts might have influenced the deconvolved measurements). Potentiated connections exhibited less transmission failures at the "after" phase than at the "before" phase, resulting in higher N_{after} values compared with N_{before}; and depressed connections exhibited more failures, resulting in lower N_{after} estimates. The estimated values gleaned from the failure analysis were remarkably similar to the estimated values from the CV analysis (Fig. 5*C*). In particular, the N_{after}/N_{before} ratio was correlated strongly with the ratio of the synaptic efficacy (with the 1st EPSP, CC = 0.7, $p < 0.001$, Fig. 5*D*; and with *A*, CC = 0.79, $p < 0.001$; data not shown, $n = 25$, t test). Hence, the failure analysis supports the conclusion that modulations in the number of release sites are a primary factor in sLTP and sLTD.

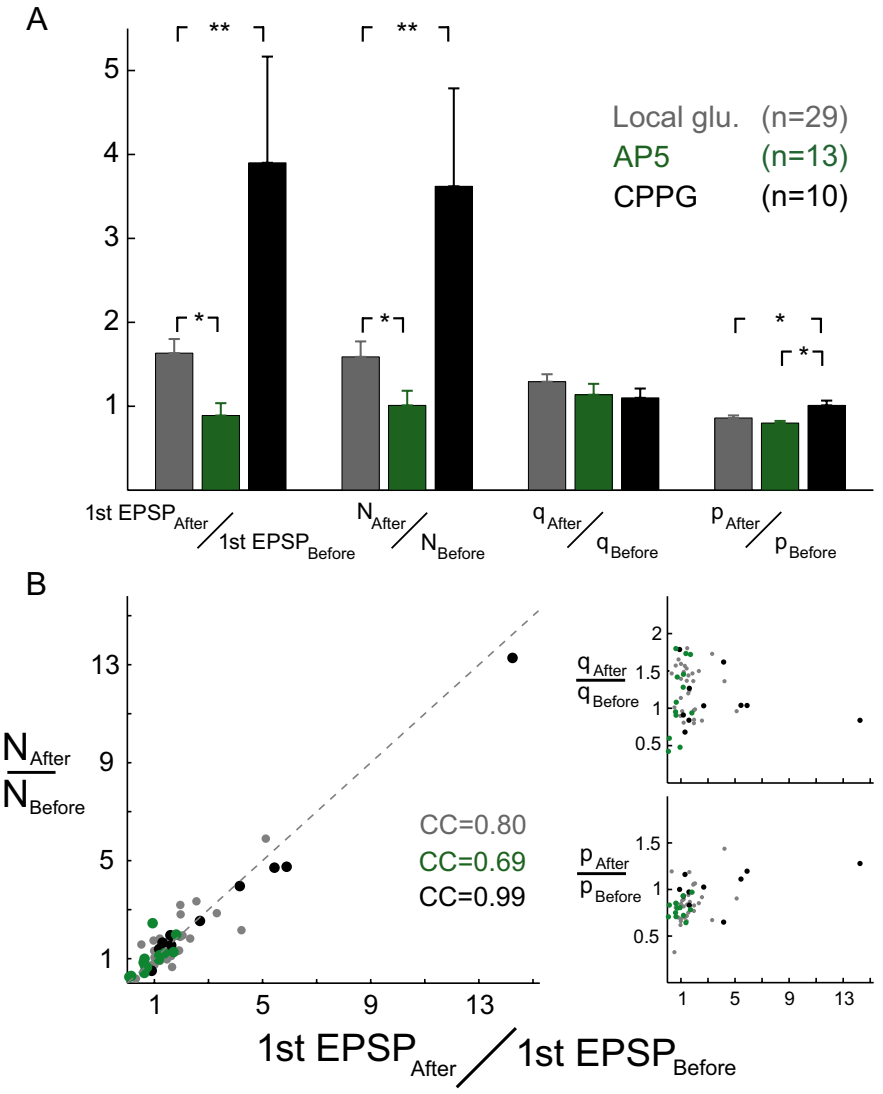

Figure 6. Facilitating or inhibiting plasticity expression does not change the mechanism underlying sLTP/sLTD. ***A***, The relative efficacy changes, estimated number of release sites, quantal size, and release probability for the experimental conditions that resulted in the largest (CPPG condition) and smallest (AP5 condition) increase in efficacy, and comparing them with the Local glutamate condition. Values are mean ± SEM. Significance was calculated with two-sample t test. ***B***, Although different in degree of expression, plotting the ratios of the quantal parameters from the "before" and "after" phases of measurements versus the changes in response efficacy reveals that the underlying processes involved remained similar at the different experimental conditions.

The co-dependency of the presynaptic and postsynaptic components of sLTP/sLTD

To further examine the co-dependency between the presynaptic changes in N and the associated postsynaptic changes, we analyzed the sLTP/sLTD induced under various experimental conditions (see Materials and Methods). As shown by Le Bé and Markram (2006), the average change in synaptic efficacy depends on the spiking activity in the slice during the 12 h window between "before" and "after," with a larger increase during the Local glutamate conditioning compared with the Global glutamate and Control experiment. The Local glutamate condition ensured a better synchronization between the neurons with the glutamate

Table 1. Measured and estimated average synaptic parameters as found at the "before" phase of the local glutamate, AP5, and CPPG experimental conditions[a]

	Local glutamate ($n = 29$)	AP5 ($n = 13$)	CPPG ($n = 10$)
First EPSP amplitude (mV)	1.81 ± 1.32	1.87 ± 1.32	1.24 ± 1.08
A (mV)	4.35 ± 3.58	3.72 ± 2.65	2.33 ± 1.8
N	46 ± 40	34 ± 18	25 ± 18
p	0.45 ± 0.1	0.48 ± 0.08	0.51 ± 0.1
q (mV)	0.1 ± 0.04	0.11 ± 0.07	0.1 ± 0.02
τ_{rec} (ms)	460 ± 132	445 ± 99	462 ± 128

[a]Values are mean ± SD. For all parameters, the differences of the values were nonsignificant between the different conditions.

puffed in a controlled manner (Le Bé and Markram, 2006, their Fig. 1), whereas the firing of the neurons in the Control or Global glutamate conditions was more random. The changes that underlie the synaptic sLTP and sLTD are, however, the same with or without glutamate as shown by the significant correlation between N_{after}/N_{before} and 1st $EPSP_{after}$/1st $EPSP_{before}$ (Control, CC = 0.81, $p < 0.001$, $n = 18$; "Evoked 1," CC = 0.80, $p < 0.001$, $n = 29$), indicating that glutamate is only enhancing a phenomenon that already exists in spontaneously active neural circuits.

The average increase in efficacy also depends on glutamate AMPA, NMDA, and mGluR5 receptor activation and on group III mGluRs but is independent on group II mGluR activation (Le Bé and Markram, 2006). These observations may result from two main alternative scenarios. In the first scenario, interfering with one of the components underlying the synaptic plasticity reduces the average increase in efficacy, without affecting the expression of the other component. For example, blocking NMDA channels may affect the addition of postsynaptic receptors, but not the addition of presynaptic release sites, leading to a uniform decrease in quantal size. Another possibility is that the changes to the presynaptic and postsynaptic components always occur in accordance, and interfering with a necessary mechanism for the expression of one component will also prevent the expression of the other mechanism. Our analysis strongly points toward the latter alternative. In Figure 6, we show the analyses for the cases in which the largest and smallest average changes were observed, that is, the Local glutamate condition in the presence of the group III mGluR antagonist CPPG (1st $EPSP_{after}$/1st $EPSP_{before}$ = 3.9 ± 1.26, mean ± SEM, $n = 10$), and in the presence of the NMDA receptors antagonist AP5 (1st $EPSP_{after}$/1st $EPSP_{before}$ = 0.89 ± 1.15, mean ± SEM, $n = 13$). Finally, we compare these cases with the analysis of the connections from Local glutamate (1st $EPSP_{after}$/1st $EPSP_{before}$ = 1.71 ± 0.19, mean ± SEM, $n = 29$). The synapses analyzed at the different conditions had similar response amplitudes, variability, and short-term dynamics in the "before" phase, which was reflected in the synaptic parameters (Table 1). In the "after" phase, a larger fraction of the connections at the AP5 experiments exhibited sLTD, whereas a smaller fraction exhibited sLTD at the CPPG condition (AP5, 8 of 13; CPPG, 1 of 10; Local glutamate, 6 of 29). The potentiation of the remaining connections was smaller in the AP5 experiments (AP5, 1.44 ± 0.13, $n = 5$; Local glutamate, 1.97 ± 0.21, $n = 23$, mean ± SEM), and significantly larger at the CPPG condition (CPPG, 4.23 ± 1.31, $n = 9$, mean ± SEM, $p < 0.05$, two-

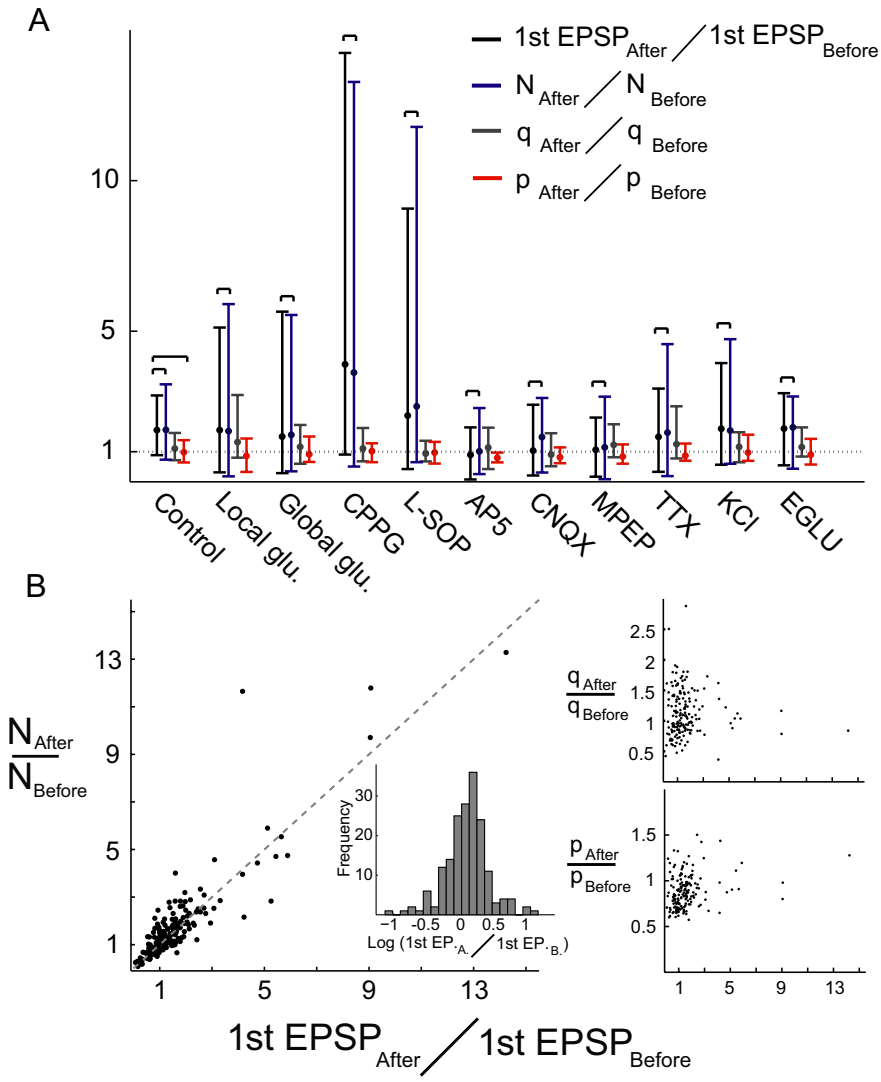

Figure 7. The codependency of the presynaptic and postsynaptic components of sLTP/sLTD is similar despite large differences in experimental conditionings. ***A***, A significant correlation between the changes in efficacy and number of release sites was found in all experimental conditions (horizontal brackets). In addition, only the changes in the number of release sites had the same range as the sLTP and sLTD. The quantal size and release probability were not correlated with efficacy changes (except the Control condition in which changes in *p* were correlated with the efficacy changes), and they fluctuated only moderately in all conditions. Upper and lower ends of each bar represent the maximum and minimum values of the respective ratios that were found, or estimated. Filled circles represent the ratio's average. ***B***, Grouping the data points from the different experimental conditions where N_{after}/N_{before} was correlated strongly with the changes in efficacy, and p_{after}/p_{before} and q_{after}/q_{before} were not, reveals the extent of the relations between the quantal parameters and sLTP or sLTD. The increase, or decrease, in the estimated number of release sites *N* follows the modulations in the synaptic efficacy for the whole range of sLTP or sLTD that we measured (0.08 < 1st $EPSP_{after}$/1st $EPSP_{before}$ < 14). Inset, Distribution of 1st $EPSP_{after}$/1st $EPSP_{before}$, depicted on a logarithmic scale for clarity. Mean and SD of this ratio are 1.63 ± 1.6. Shown are the synaptic connections from the following experimental conditions (see Materials and Methods): Local glutamate, $n = 29$; Global glutamate, $n = 34$; CPPG, $n = 10$; LSOP, $n = 18$; AP5, $n = 13$; CNQX, $n = 25$; MPEP, $n = 14$; TTX, $n = 11$; KCl, $n = 11$; EGLU, $n = 12$.

sample *t* test). Despite these differences in the expression of sLTP/sLTD at the three experimental conditions, sLTP was always explained by an increase in the number of release sites and sLTD was explained by a decrease in *N*. In particular, in all cases, the changes in the number of release sites were significantly correlated with the changes in synaptic efficacy (AP5, CC = 0.69, $p < 0.01$, $n = 13$; CPPG, CC = 0.99, $p < 0.01$, $n = 10$; *t* test). The quantal sizes, on the other hand, were similar in both measurements phases (AP5, $q_{after}/q_{before} = 1.13 \pm 0.13$, $n = 13$; CPPG, $q_{after}/q_{before} = 1.1 \pm 0.11$, $n = 10$; Local glutamate, $q_{after}/q_{before} = 1.31 \pm 0.08$, $n = 29$, mean ± SEM; Fig. 6).

The analysis from the other experimental conditions reveals a similar picture, that is, although the expression of sLTP/sLTD can depend on key synaptic components, the underlying presynaptic and postsynaptic quantal modulations of the changes in efficacy remained matched: the N_{after}/N_{before} ratio was correlated with, and had the same relative range as, the changes in the synaptic efficacy (CNQX, CC = 0.87, $p < 0.001$, $n = 25$; TTX, CC = 0.73, $p < 0.05$, $n = 11$; MPEP, CC = 0.98, $p < 0.001$, $n = 14$; LSOP, CC = 0.97, $p < 0.001$, $n = 18$; EGLU, CC = 0.65, $p < 0.05$, $n = 12$; KCl, CC = 0.87, $p < 0.001$, $n = 11$; *t* test), and q_{after}/q_{before} exhibited only a limited range that was centered close to unity with no correlation to the observed sLTP/sLTD (Fig. 7*A*). We found this strong codependency for the whole range of observed sLTP/LTD (i.e., from synaptic efficacies that decreased to <10% of their initial value, to synapses that strengthened by a factor of 14) (Fig. 7*B*).

Homeostatic features of sLTP and sLTD

Our findings suggest that the processes underlying the observed sLTP and sLTD are similar, with one being a mere mirror image of the other. Both forms of synaptic plasticity differed, however, by their dependency on the initial synaptic efficacy: weaker connections had a much larger potentiation range than stronger connections, whereas a dependency on the initial efficacy was not observed for the extent of sLTD (Fig. 8*A*). We also found that potentiated connections were initially weaker than those that would eventually depress ($p < 0.01$; Fig. 8*B*). These properties were captured fully by the changes in the number of release sites. Changes in *p* and *q* were uncorrelated with the initial efficacy; and the average values of both parameters were similar at potentiated and depressed connections (Fig. 8*A*,*B*). The release probability and quantal size were, however, negatively correlated with their own initial values (e.g., at synapses with initial quantal size larger than average it tended to decrease by the "after" measurement) (Fig. 8*C*).

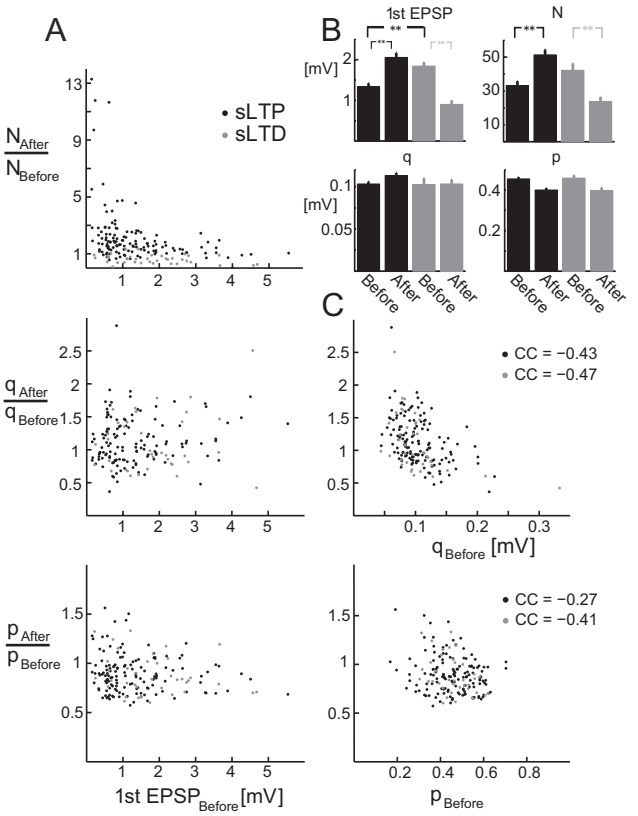

Figure 8. Homeostatic features of sLTP and sLTD. ***A***, Top, The smaller the initial efficacy, the larger the range of sLTP and the subsequent change in *N*. No such relation was found for sLTD. Changes in *p* and *q* (during sLTP and sLTD) did not depend on the initial efficacy (middle and bottom). ***B***, The average initial efficacy of the connections that eventually potentiated was significantly smaller than those who depressed ($p < 0.01$). This result was reflected in the average number of release sites, whereas *p* and *q* were similar at the potentiated and depressed connections. sLTP, $n = 139$; sLTD, $n = 38$. Error bars indicate SEM. ***C***, Changes in *p* and *q* were negatively correlated with their own initial values ($p < 0.05$ for *p* and *q*, at sLTP and sLTD).

Discussion

This study presents the first quantal and failure analyses of changes in synaptic transmission resulting from extended periods of ongoing neural activity, providing new insights into the nature of long-term synaptic plasticity. In particular, our results show that, over long time scales, the potentiation and depression of synaptic efficacies are the result of matched presynaptic and postsynaptic modifications. Three key synaptic properties did not change over the 12 hour period of the experimental paradigm: the short-term depression dynamics, the CV-mean relation, and the decrease in number of failures at stronger connections. Therefore, the large range of observed synaptic efficacies is explained at both "before" and "after" with the same relation between the number of release sites and connection strength, whereas the release probability and quantal size showed much narrower ranges of values that were uncorrelated with the efficacies (Fig. 4*A*). With similar release probabilities, the changes in efficacy and the complementary shifts along the CV-mean relation observed at specific synaptic connections are consistent with proportional changes in the number of release sites and a constant quantal size. Our findings are thus in line with studies focusing on synaptic plasticity at shorter time scales (Lisman and Raghavachari, 2006; Redondo and Morris, 2011) and corroborate the hypothesis that long-term potentiation has a modular cross-synaptic nature. We also show that long-term depression exhibits the same characteristic features. This suggests that sLTP and sLTD represent two opposite manifestations of one functionally unified underlying process for modulating synaptic efficacies.

Our findings bridge the gap between known structural synaptic plasticity and the unknown changes that occur at the microstructural level, which are inaccessible using current imaging techniques. Spine volumes increase after LTP and decrease after LTD (Matsuzaki et al., 2004; Zhou et al., 2004; Yang et al., 2008); and based on our analysis, we predict that these volume changes are tightly associated with comparable changes in the volumes of the correspondent presynaptic boutons. We further predict that both volumes vary in proportion to the number of functional transmission modules that are added or subtracted. This prediction is supported by the observation that the dependency between the number of added transmission modules and a

connection's initial efficacy (Fig. 8*A*) is remarkably similar to the dependency between the increase in spine volume and its initial volume after sustained neural activity (Yasumatsu et al., 2008). Our finding that the level of depression was not correlated with the initial efficacy also compare with the properties of decreasing spine volumes (Yasumatsu et al., 2008). Although it is reasonable to assume that transmission modules at depressed connections are removed from existing synaptic contacts, our analysis does not tell whether new transmission modules at potentiated connections are added at existing, or at newly formed, synaptic contacts. The similarity of the short-term dynamics of new, existing, and potentiated connections (Le Bé and Markram, 2006) suggests that the modular modification is operant in all cases. Still, the strong dependency of sLTP, but not the appearance of new connections, on AMPA and NMDA receptor activation (Le Bé and Markram, 2006) (Fig. 7) indicates that the majority of new transmission modules were added at existing synaptic contacts. This interpretation is in agreement with three anatomical findings: (1) cortical spines have a growth potential that span a similar two-order of magnitudes as synaptic efficacies (Knott et al., 2006); (2) larger postsynaptic densities face larger active zones with more docked vesicles (Schikorski and Stevens, 1997, 1999); and (3) excitatory synaptic contacts on layer-5 basal dendrites can include several active zones of different sizes with increasing number of docked vesicles at the larger ones (Rollenhagen and Lübke, 2006). Functionally, the mechanism of strengthening a synaptic connection by the addition of transmission modules at existing contacts emphasizes their specific dendritic location, which has a strong effect on the computation performed by the dendrites (Segev and London, 2000; Gulledge et al., 2005; London and Häusser, 2005). Nonetheless, the addition of new contacts at different dendritic locations represents a vital complementary mechanism to the potentiation of existing contacts, with which new functional facets can be explored and supplemented to the interaction between already connected cells. Moreover, as new spines are associated with boutons of comparable volume (Knott et al., 2006), our findings may hold for new contact points as well.

The new transmission modules at potentiated synapses shared similar quantal sizes and release probabilities with the modules that already existed in the "before" phase, even at connections in which the added modules outnumbered existing modules by several-fold. These quantal parameters were not a factor in determining the subtraction of modules during sLTD. The relatively narrow range of quantal sizes may reflect a combination of two phenomena: (1) synaptic contacts between layer-5 pyramidal neurons are predominantly located at basal dendrites, with a narrow range of electrotonic distance from the soma (Markram et al., 1997); and (2) quantal sizes are expected to be of stereotypical magnitude resulting from anatomical and functional constraints (Raghavachari and Lisman, 2004). The release probabilities had a similarly narrow range than that of the changes in the efficacies, which result from the initial average value of ~0.5 and from the constrained range of the release probability, which can only take values between zero and unity. However, the observed changes in the release probabilities were of magnitudes that affect the temporal coding properties of synapses (e.g., by modulating their dynamic gain control) (Abbott et al., 1997) and by changing their sensitivity to temporal coherence (Tsodyks and Markram, 1997). The fact that the changes in p were uncorrelated with the changes in efficacy suggests that the two alternatives for modifying the synaptic responses are generated by different plasticity rules. All together, ongoing neural activity leads to matched changes in the amount of presynaptic and postsynaptic resources at existing connections, to the rewiring of neuronal circuits via the appearances and disappearances of synaptic connections (Le Bé and Markram, 2006), and to the redistribution of the resources' utilization to spike trains stimuli (Tsodyks and Markram, 1997; Sjöström et al., 2007).

The exponents of the CV-mean relations were remarkably similar to the value of -0.5 predicted from the quantal model for the case in which the different efficacies are determined by changes in the number of transmission modules (Fig. 3). Exponents deviating from -0.5 predict different correlations between p, q, and the efficacies, e.g., values >-0.5, indicate a possible increase of the quantal size at synapses with larger efficacies, whereas smaller exponents indicate a possible increase in the release probability. Comparing the exponents we found for the layer-5 connections with those of CV-mean relations at other connection types will therefore indicate to what extent changes in the number of transmission modules explain their efficacy range as well. Indeed, the key features of a wide efficacy distribution with decreasing CV-mean relation are repeatedly observed at cortical synaptic connections between various cell types at different layers (Feldmeyer et al., 1999, 2002, 2006; Lefort et al., 2009), although their exponents, to our knowledge, have yet to be calculated. How diverse the exponent values are will also indicate to how diverse are the plasticity rules that determine synaptic plasticity that follows ongoing neural activity. Interestingly, although functional roles for the observed wide distributions (i.e., maximizing storage capacity) (Brunel et al., 2004) and for the stochastic nature of synaptic transmission (in learning) (Seung, 2003), and for maximizing information transmission under the constraint of limited resources (Levy and Baxter, 2002; Schreiber et al., 2002; Goldman, 2004) have been suggested separately, the functional significance of the stereotypical CV-mean combined relation observed at numerous synaptic populations is unknown. Exploring the role of these relations in neural coding and revealing the underlying plasticity rules present a combined experimental and theoretical challenge to our understanding of the function of neuronal circuits.

References

Abbott L, Varela J, Sen K, Nelson S (1997) Synaptic depression and cortical gain control. Science 275:221–224. CrossRef Medline

Bayazitov IT, Richardson RJ, Fricke RG, Zakharenko SS (2007) Slow presynaptic and fast postsynaptic components of compound long-term potentiation. J Neurosci 27:11510–11521. CrossRef Medline

Bolshakov VY, Golan H, Kandel ER, Siegelbaum SA (1997) Recruitment of new sites of synaptic transmission during the cAMP-dependent late phase of LTP at CA3–CA1 synapses in the hippocampus. Neuron 19:635–651. CrossRef Medline

Brunel N, Hakim V, Isope P, Nadal JP, Barbour B (2004) Optimal information storage and the distribution of synaptic weights: perceptron versus Purkinje cell. Neuron 43:745–757. CrossRef Medline

Debanne D, Guérineau NC, Gähwiler B, Thompson SM (1996) Paired-pulse facilitation and depression at unitary synapses in rat hippocampus: quantal fluctuation affects subsequent release. J Physiol 491:163–176. Medline

Del Castillo J, Katz B (1954) Quantal components of the end-plate potential. J Physiol 124:560–573. Medline

Efron B, Tibshirani RJ (1993) An introduction to the bootstrap. London: Chapman and Hall.

Feldmeyer D, Egger V, Lübke J, Sakmann B (1999) Reliable synaptic connections between pairs of excitatory layer 4 neurones within a single "barrel" of developing rat somatosensory cortex. J Physiol 521:169–190. CrossRef Medline

Feldmeyer D, Lübke J, Silver RA, Sakmann B (2002) Synaptic connections between layer 4 spiny neurone-layer 2/3 pyramidal cell pairs in juvenile

rat barrel cortex: physiology and anatomy of interlaminar signalling within a cortical column. J Physiol 538:803–822. CrossRef Medline

Feldmeyer D, Lübke J, Sakmann B (2006) Efficacy and connectivity of intracolumnar pairs of layer 2/3 pyramidal cells in the barrel cortex of juvenile rats. J Physiol 575:583–602. CrossRef Medline

Fuhrmann G, Segev I, Markram H, Tsodyks M (2002) Coding of temporal information by activity-dependent synapses. J Neurophysiol 87:140–148. Medline

Gardiner CW (1983) Handbook of stochastic methods. Berlin: Springer.

Goelet P, Castellucci VF, Schacher S, Kandel ER (1986) The long and the short of long-term memory: a molecular framework. Nature 322:419–422. CrossRef Medline

Goldman MS (2004) Enhancement of information transmission efficiency by synaptic failures. Neural Comput 16:1137–1162. CrossRef Medline

Gulledge AT, Kampa BM, Stuart GJ (2005) Synaptic integration in dendritic trees. J Neurobiol 64:75–90. CrossRef Medline

Hebb DO (1949) The organization of behavior: a neuropsychological theory. New York: Wiley.

Isope P, Barbour B (2002) Properties of unitary granule cell→Purkinje cell synapses in adult rat cerebellar slices. J Neurosci 22:9668–9678. Medline

Knott GW, Holtmaat A, Wilbrecht L, Welker E, Svoboda K (2006) Spine growth precedes synapse formation in the adult neocortex in vivo. Nat Neurosci 9:1117–1124. CrossRef Medline

Le Bé JV, Markram H (2006) Spontaneous and evoked synaptic rewiring in the neonatal neocortex. Proc Natl Acad Sci U S A 103:13214–13219. CrossRef Medline

Lefort S, Tomm C, Floyd Sarria JC, Petersen CC (2009) The excitatory neuronal network of the C2 barrel column in mouse primary somatosensory cortex. Neuron 61:301–316. CrossRef Medline

Levy WB, Baxter RA (2002) Energy-efficient neuronal computation via quantal synaptic failures. J Neurosci 22:4746–4755. Medline

Lisman J, Raghavachari S (2006) A unified model of the presynaptic and postsynaptic changes during LTP at CA1 synapses. Sci STKE 2006:re11. CrossRef Medline

Loebel A, Silberberg G, Helbig D, Markram H, Tsodyks M, Richardson MJ (2009) Multiquantal release underlies the distribution of synaptic efficacies in the neocortex. Front Comput Neurosci 3:27. CrossRef Medline

London M, Häusser M (2005) Dendritic computation. Annu Rev Neurosci 28:503–532. CrossRef Medline

Markram H, Lübke J, Frotscher M, Roth A, Sakmann B (1997) Physiology and anatomy of synaptic connections between thick tufted pyramidal neurones in the developing rat neocortex. J Physiol 500:409–440. Medline

Martin SJ, Grimwood PD, Morris RG (2000) Synaptic plasticity and memory: an evaluation of the hypothesis. Annu Rev Neurosci 23:649–711. CrossRef Medline

Matsuzaki M, Ellis-Davies GC, Nemoto T, Miyashita Y, Iino M, Kasai H (2001) Dendritic spine geometry is critical for AMPA receptor expression in hippocampal CA1 pyramidal neurons. Nat Neurosci 4:1086–1092. CrossRef Medline

Matsuzaki M, Honkura N, Ellis-Davies GC, Kasai H (2004) Structural basis of long-term potentiation in single dendritic spines. Nature 429:761–766. CrossRef Medline

Raghavachari S, Lisman JE (2004) Properties of quantal transmission at CA1 synapses. J Neurophysiol 92:2456–2467. CrossRef Medline

Ramón y Cajal S (1899) Textura del sistema nervioso del hombre y de los vertebrados: estudios sobre el plan estructural y composición histológica de los centros nerviosos adicionados de consideraciones fisiológicas fundadas en los nuevos descubrimentos. Madrid: Moya.

Redondo RL, Morris RG (2011) Making memories last: the synaptic tagging and capture hypothesis. Nat Rev Neurosci 12:17–30. CrossRef Medline

Richardson MJ, Silberberg G (2008) Measurement and analysis of postsynaptic potentials using a novel voltage-deconvolution method. J Neurophysiol 99:1020–1031. CrossRef Medline

Richardson MJ, Melamed O, Silberberg G, Gerstner W, Markram H (2005) Short-term synaptic plasticity orchestrates the response of pyramidal cells and interneurons to population bursts. J Comput Neurosci 18:323–331. CrossRef Medline

Rollenhagen A, Lübke JH (2006) The morphology of excitatory central synapses: from structure to function. Cell Tissue Res 326:221–237. CrossRef Medline

Schikorski T, Stevens CF (1997) Quantitative ultrastructural analysis of hippocampal excitatory synapses. J Neurosci 17:5858–5867. Medline

Schikorski T, Stevens CF (1999) Quantitative fine-structural analysis of olfactory cortical synapses. Proc Natl Acad Sci U S A 96:4107–4112. CrossRef Medline

Schreiber S, Machens CK, Herz AV, Laughlin SB (2002) Energy-efficient coding with discrete stochastic events. Neural Comput 14:1323–1346. CrossRef Medline

Segev I, London M (2000) Untangling dendrites with quantitative models. Science 290:744–750. CrossRef Medline

Seung HS (2003) Learning in spiking neural networks by reinforcement of stochastic synaptic transmission. Neuron 40:1063–1073. CrossRef Medline

Shepherd JD, Huganir RL (2007) The cell biology of synaptic plasticity: AMPA receptor trafficking. Annu Rev Cell Dev Biol 23:613–643. CrossRef Medline

Silver RA, Momiyama A, Cull-Candy SG (1998) Locus of frequency-dependent depression identified with multiple-probability fluctuation analysis at rat climbing fibre-Purkinje cell synapses. J Physiol 510:881–902. CrossRef Medline

Sjöström PJ, Turrigiano GG, Nelson SB (2007) Multiple forms of long-term plasticity at unitary neocortical layer 5 synapses. Neuropharmacology 52:176–184. CrossRef Medline

Südhof TC, Malenka RC (2008) Understanding synapses: past, present, and future. Neuron 60:469–476. CrossRef Medline

Thomson AM, Deuchars J, West DC (1993) Large, deep layer pyramid-pyramid single axon EPSPs in slices of rat motor cortex display paired pulse and frequency-dependent depression, mediated presynaptically and self-facilitation, mediated postsynaptically. J Neurophysiol 70:2354–2369. Medline

Tsodyks MV, Markram H (1997) The neural code between neocortical pyramidal neurons depends on neurotransmitter release probability. Proc Natl Acad Sci U S A 94:719. CrossRef Medline

Varela JA, Sen K, Gibson J, Fost J, Abbott LF, Nelson SB (1997) A quantitative description of short-term plasticity at excitatory synapses in layer 2/3 of rat primary visual cortex. J Neurosci 17:7926–7940. Medline

Yang Y, Wang XB, Frerking M, Zhou Q (2008) Spine expansion and stabilization associated with long-term potentiation. J Neurosci 28:5740–5751. CrossRef Medline

Yasumatsu N, Matsuzaki M, Miyazaki T, Noguchi J, Kasai H (2008) Principles of long-term dynamics of dendritic spines. J Neurosci 28:13592–13608. CrossRef Medline

Zhou Q, Homma KJ, Poo MM (2004) Shrinkage of dendritic spines associated with long-term depression of hippocampal synapses. Neuron 44:749–757. CrossRef Medline

Zucker RS, Regehr WG (2002) Short-term synaptic plasticity. Annu Rev Physiol 64:355–405. CrossRef Medline